Report of Test

Absolute Spectral Radiance Responsivity

of the

NASA GLAMR exIGA Radiometer
L-1 model 8350, S/N 002

Request Submitted by:

Joel McCorkle
NASA Goddard Space Flight Center
Greenbelt, MD

1. Description of Calibration Items

The device under test (DUT) is an extended-InGaAs radiance meter manufactured by L-1 Standards and Technology, Inc. (L-1), model 8350, S/N 002. The device is housed in a 2 inch diameter tube with a fore-optic consisting of an aperture and lens. The detector is temperature controlled (L-1 model 3100-1L, S/N 12132) and the rear of the device has inputs for the L-1 temperature controller and a BNC output for the detector signal. The detector came with an L-1 model 3300v2, S/N 008, transimpedance amplifier which was used for the calibration.

1.1 Calibration Request

We were requested to calibrate the instrument for absolute radiance responsivity from 1600 nm to 2500 nm.

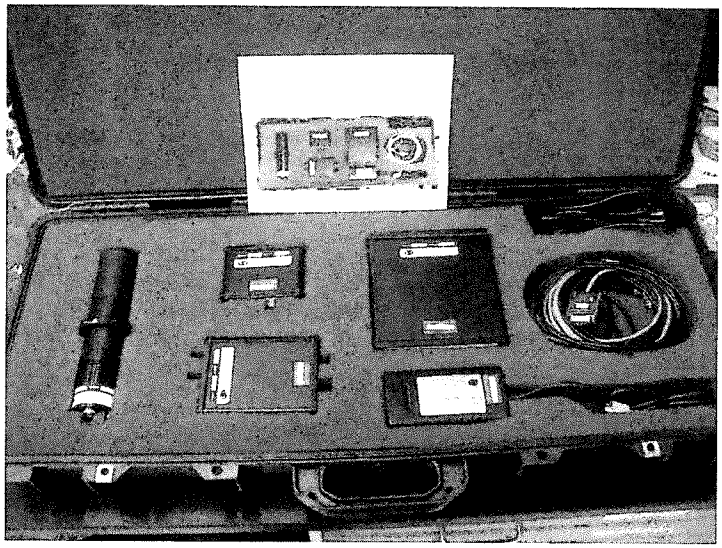

Figure 1.1. Picture of GLAMR exIGA Radiometer.

2. Description of Test

The detector was characterized for absolute spectral radiance responsivity on the NIST facility for Spectral Irradiance and Radiance responsivity Calibrations using Uniform Sources (SIRCUS).[1,2] The calibration took place from Sept. 1, 2018 to Sept. 25, 2018. During the test the detector was temperature controlled at -20.0 °C by the L-1 controller and checked at the beginning and end of each calibration session. The calibration was performed in four parts: a relative measurement of power responsivity was performed vs. a Gentec pyroelectric sensor from 1250 nm to 2200 nm, an absolute radiance responsivity measurement from 1300 nm to 1600 nm, a relative radiance responsivity vs. the pyroelectric sensor from 1925 nm to 2500 nm, and a reflectance measurement of the pyroelectric sensor.

2.1 Relative Power Responsivity (1250 nm to 2200 nm)

The spectral power responsivity of the DUT from 1250 nm to 2200 nm was measured relative to that of a pyroelectric detector which has a relatively flat spectral response.

$$\frac{S_{DUT}(\lambda)}{S_{pyro}(\lambda)} = K(\lambda)$$

The measurement was performed using a chopped beam from an IR monochromator with a supercontinuum laser source. The beam, chopped at 10 Hz, is about 1.5 mm in diameter and with a bandwidth of about 1.5 nm. The pyroelectric detector (abbreviated as "pyro") is from Gentec and has an active area of 5 mm in diameter. The responses of the DUT and the pyroelectric detector were measured in sequence with a translation stage which transported each detector such that the incident light beam was positioned, with a normal incidence, in the center of the active area of the detector of interest. During measurement of each detector, an external, extended-InGaAs detector monitored any fluctuation of the probing beam through a beam splitter placed in the optical path. The spectral response of each detector was subsequently normalized by the monitor signal.

2.2 Pyroelectric Detector Reflectance

The spectral response of a pyroelectric detector is typically flat but subject to small variations that arise from the change in the reflectance from the diffused scattering of the organic black coating of the pyroelectric detector. A correction for reflectance change is needed to reduce the uncertainty. The spectral reflectance as a function of wavelength, $R(\lambda)$, from the pyroelectric detector was measured separately from the power responsivity measurement by using a 3 mm diameter, temperature stabilized, extended-InGaAs detector. The measurement was performed in two steps. First, the reflectance measuring photodiode was positioned such that the light beam was incident in the center of the active area with a normal incidence. The spectral response of the photodiode was then recorded. Second, the reflectance measuring photodiode was repositioned to face the pyroelectric detector at 10 cm distance from the pyroelectric detector and about 30 degrees from the normal. For this measurement, the light beam was directed to the center of the pyroelectric detector with a normal incidence and the spectral response of the reflectance measuring photodiode, which measured the scattered light from the pyroelectric detector, was recorded. After the above two measurements, the pyroelectric detector reflectance was determined

using the ratio of the responses of the two measurements and several tie points that are traceable to the additional visible measurements.

2.3 Absolute Radiance Responsivity (1300 nm to 1600 nm)

Absolute radiance responsivity measurements were performed on SIRCUS. A 50 mm (2") aperture was used on the integrating sphere source (ISS) and the IGA2017A transfer standard and the GLAMR exIGA radiance meter were aligned to the center of the aperture. Reflections from a glass slide placed across the front of each detector were used to align each instrument to the optical axis. The Precision #2 transimpedance amplifier was used with IGA2017A and the provided L-1 transimpedance amplifier was used with the GLAMR exIGA. The idler of LBO/OPO laser system was used and the Bristol 521 (SN 5018) wavemeter measured the wavelength of the signal. The source sphere was placed approximately 30 cm from the front surface of the GLAMR exIGA radiance meter. The IGA2017A reference plane was determined radiometrically – see Section 3.1.

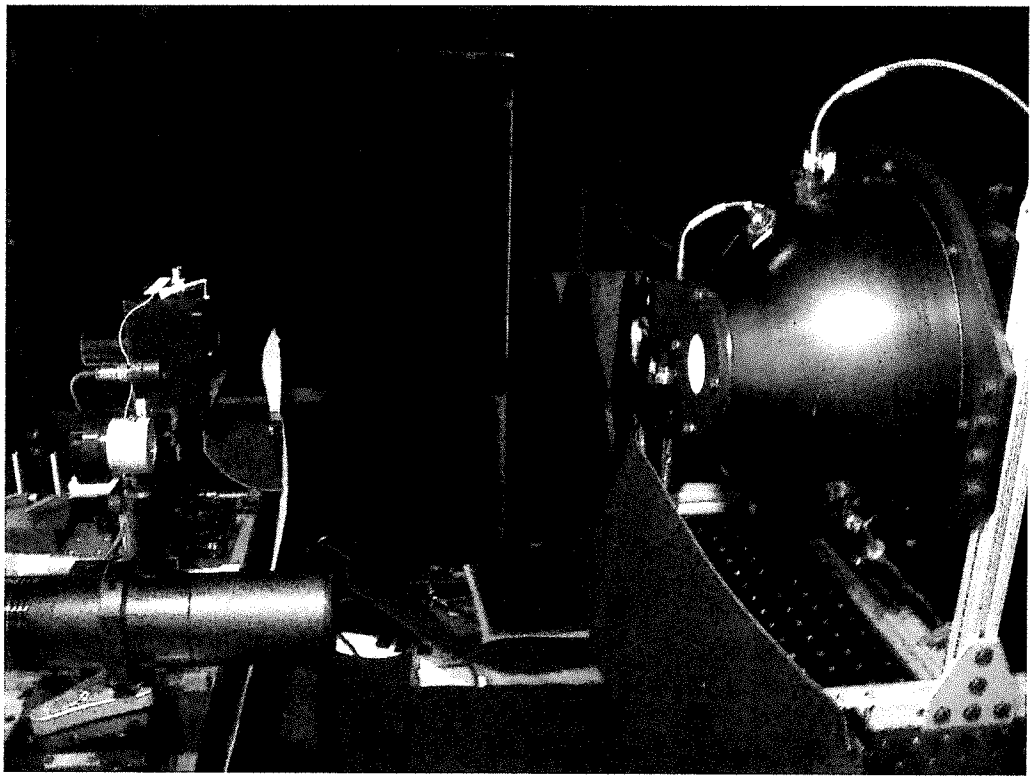

Figure 2.1. Detector bench setup.

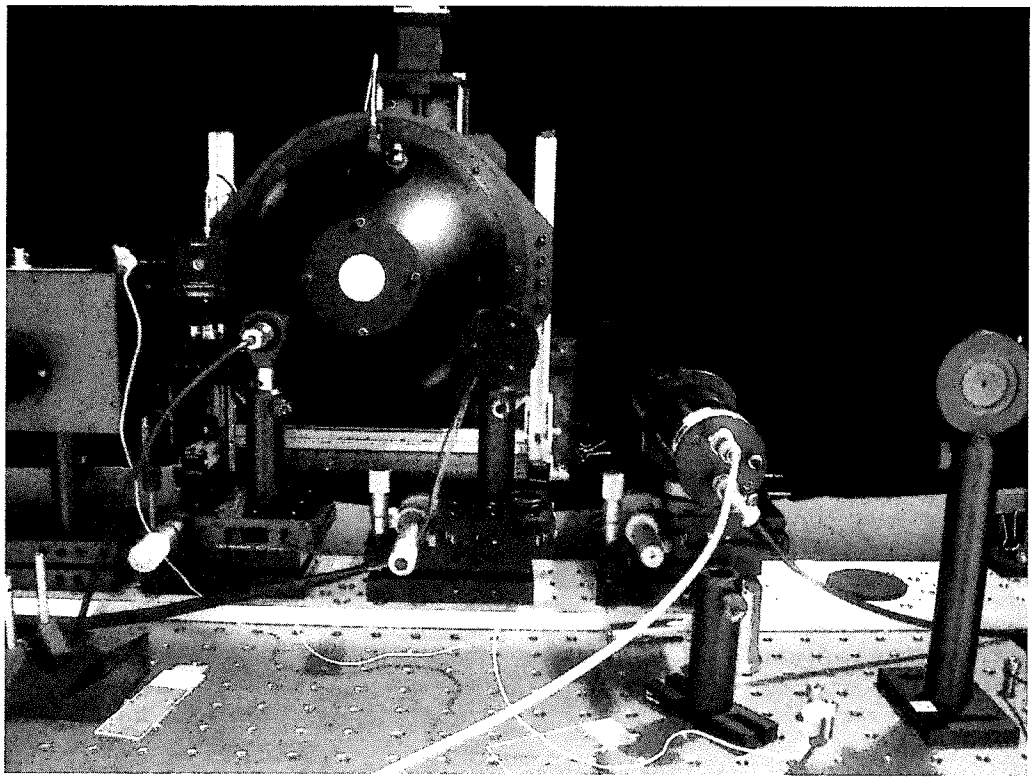

Figure 2.2. Detector bench with transfer standards (left), pyroelectric detector (center) and GLAMR radiance detector (right).

2.4 Relative Radiance Responsivity (1925 nm to 2500 nm)

For the relative radiance responsivity measurements of the L-1 exIGA detector to the pyroelectric detector, the sphere was moved to be ~15 cm from the GLAMR exIGA radiance meter and the pyroelectric detector was positioned to the side of the GLAMR exIGA and oriented toward the aperture of the sphere. A Gamma Scientific exIGA radiance meter was positioned to look in the sphere from the side and was used as sphere monitor. The source was the IPG Cr^{2+}:ZnS/Se Narrowline Tunable Laser and the wavelength was measured with a Burleigh WA-1500 (S/N 0024213).

These measurements were obtained in AC mode using an Oriel Instruments model 3502 optical chopper operating at 10 Hz. A National Instruments NI-USB 6211 data acquisition device was used to collect the digitized square waveforms (10,000 points at 10 kHz acquisition rate) from the pyroelectric detector, GLAMR exIGA radiance meter, and the exIGA sphere monitor. The transient region from each waveform was removed and the DC signal taken as the difference between the average high and low signals. The GLAMR exIGA radiance meter and pyroelectric detector signals were each normalized to the simultaneously collected monitor signal.

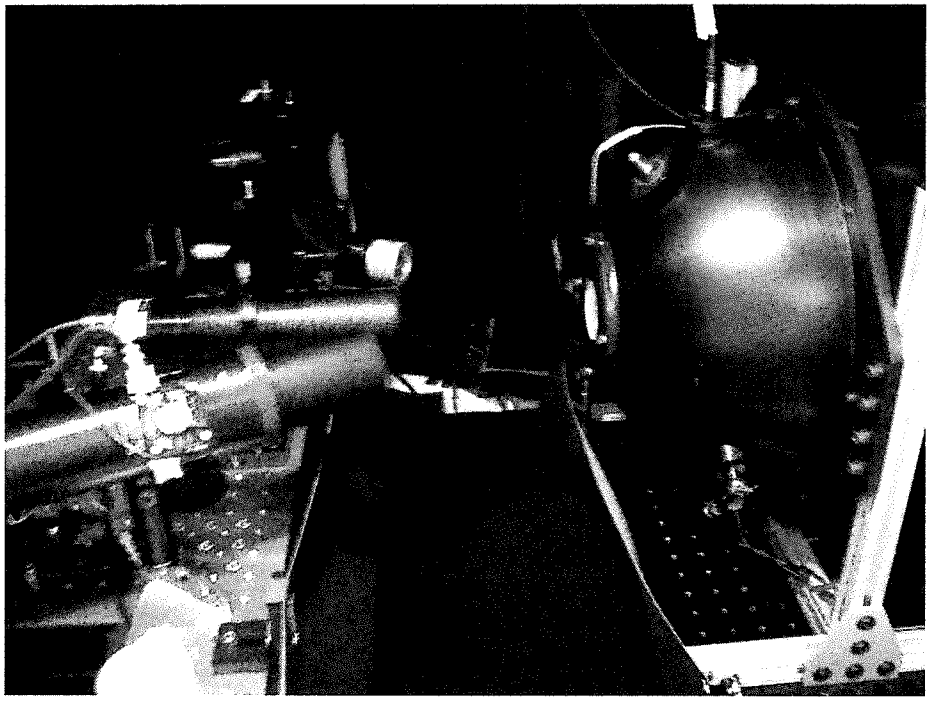

Figure 2.3. Side-view of the detector setup during the relative radiance responsivity measurements from 1900 nm to 2500 nm.

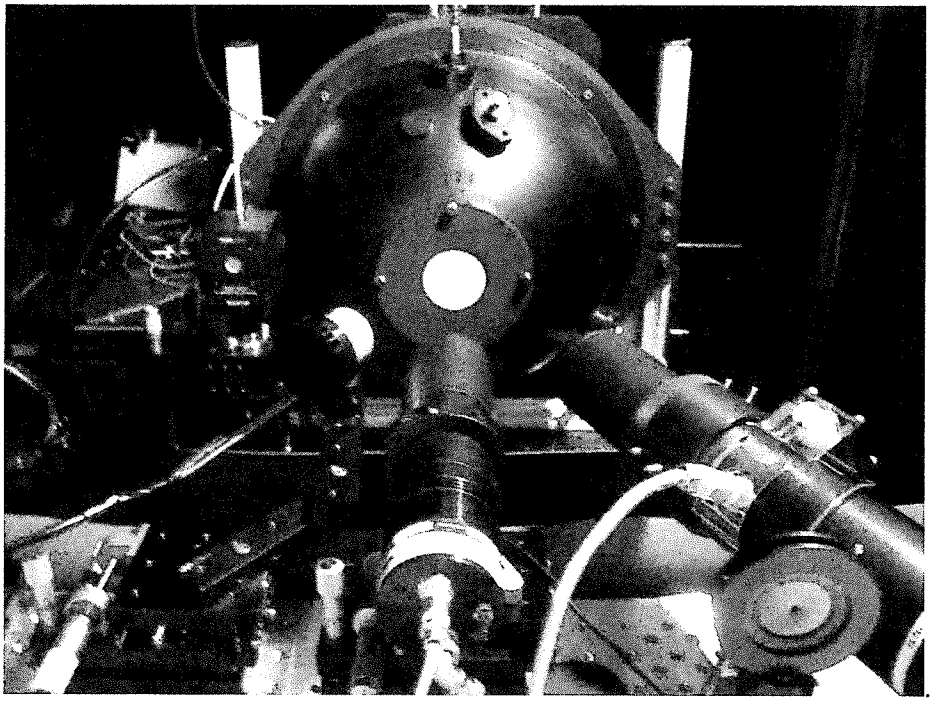

Figure 2.4. View from behind the detector bench of the detector setup during the relative radiance responsivity measurements.

3. Results of Test

The absolute radiance responsivity was measured relative to the IGA2017A transfer standard. The IGA2017A detector is an irradiance meter. To measure radiance the solid angle of the source is required. To determine the solid angle, the distance between the transfer standard aperture and the integrating sphere source aperture must be known along with the integrating sphere aperture area.

The integrating sphere is mounted on an XYZ translation stage, with the Z position measured with a linear encoder. The X and Y axes enable the source to be properly positioned in front of an instrument before it measures the sphere radiance. The Z position is used to determine the separation between relevant apertures.

3.1 Trap detector offset and offset uncertainty determination

For radiance responsivity measurements, the IGA2017A detector distance was measured radiometrically. The integrating sphere source was illuminated with 895 nm light. At ten different Z positions, the transfer standard and monitor voltages were recorded to yield a relative irradiance. From the Z position encoder reading, the actual transfer standard aperture to sphere aperture distance in millimeters was determined using the $1/Z^2$ law for on-axis irradiance (inverse square law). The resultant data were fit to a point-source geometry and a non-point-source geometry (the experimental configuration). Fig 3.1 is a schematic of the configuration. The inverse square law fitting equation was:

$$y = \frac{m_1}{(M_0 - m_2)^2} \tag{1}$$

Where y is the relative irradiance, m_1 is a fitting constant, M_0 is Z position of the integrating sphere that is read by the Z-encoder, and m_2 is the Z position of zero offset between the two apertures. The uncertainty in m_2, for the sphere position during calibration, gives the uncertainty in the distance between the two apertures.

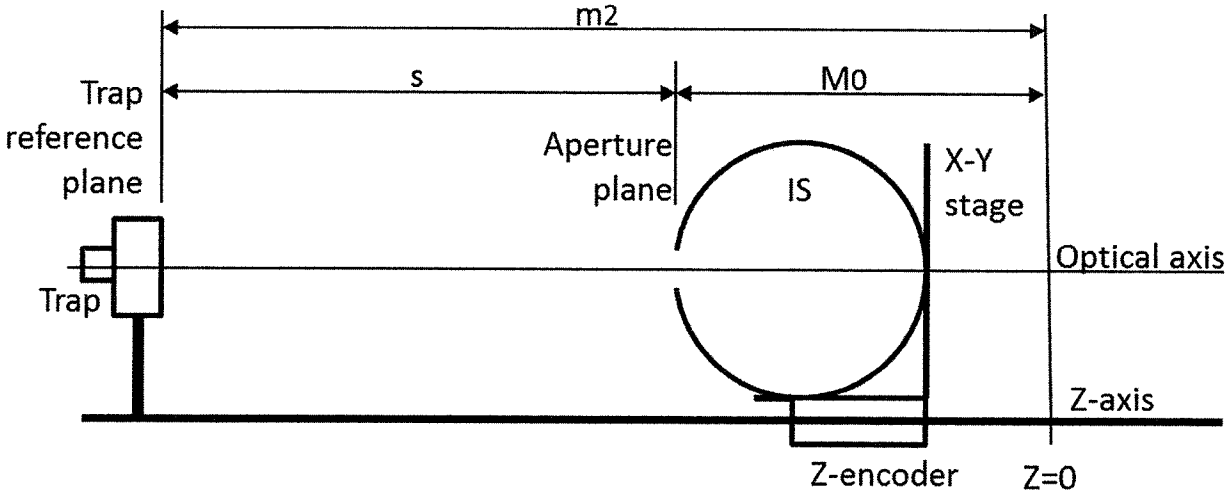

Figure 3.1. Schematic of the configuration for determining transfer standard-sphere distance radiometrically.

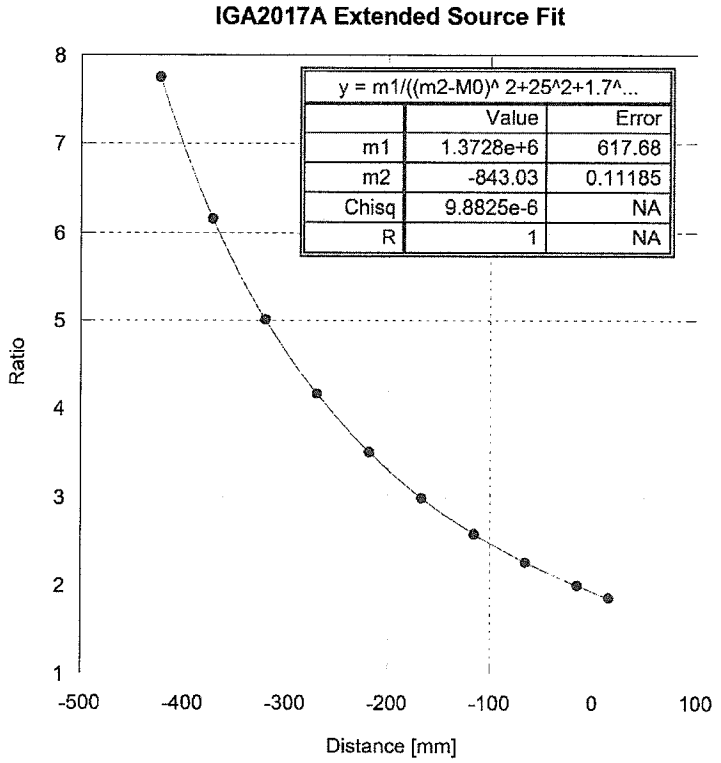

Figure 3.2. Reference IGA2017A detector offset fit to an extended aperture geometry (2).

Because the source aperture was fairly large (5.0 cm diameter), the point source approximation was tested by fitting the data to the expression:

$$y = \frac{m_1}{((M_0 - m_2)^2 + m_3^2 + m_4^2)} \tag{2}$$

where y, m_1, M_0, and m_2 are the same as in Eq. 1. $m_3 = r_d$, the radius of the trap aperture, 1.7 mm, and $m_4 = r_d$, the radius of the integrating sphere aperture, 25 mm. Expression 2 is valid in the limit where

$$\left(r_s^2 + r_d^2 + s^2\right) >> 2 r_s r_d \tag{3}$$

At a separation, s, of 40 cm, the minimum separation for the distance measurement, $(r_s^2 + r_d^2 + s^2)/2r_s r_d = 1890$, and the condition, Eq. 3, holds.

The fit to Eq. 2 has an offset, m_2, of -843.03 mm and an uncertainty of 0.11 mm. Residuals to the fit are shown in Fig. 3.3. There is no apparent bias or offset to the residuals, and the magnitude of the residuals is on the order of the resolution of the measurements themselves. Note that there is a 1.2 mm difference in m_2 between the point source and the extended source calculations. Thus, the use of Eq. 2 results in a 0.5% correction to the responsivity compared to Eq. 1. The offset, m_2 = -843.03 mm was used for the transfer standard position in the data reduction; the offset had an uncertainty of 0.11 mm.

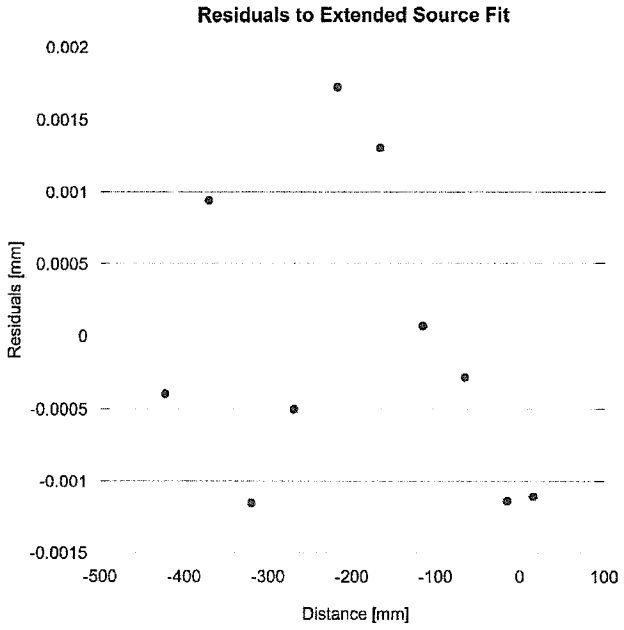

Figure 3.3. Residuals to the fit of the distance data to Eq. 2.

For data collection of the absolute radiance responsivity in the 1300 nm to 1600 nm range the ISS was placed 300.0 mm from the front aperture of the exIGA radiometer DUT as measured with a Mitutoyo ruler. This corresponded to a z position of -392.67 mm or approximately 450 mm from the transfer standard detector. A plot of the response of the exIGA radiometer vs. distance from the front aperture is shown in Fig. 3.4. In the range around a 300 mm separation there is no change in response with distance as required for a valid radiance measurement.

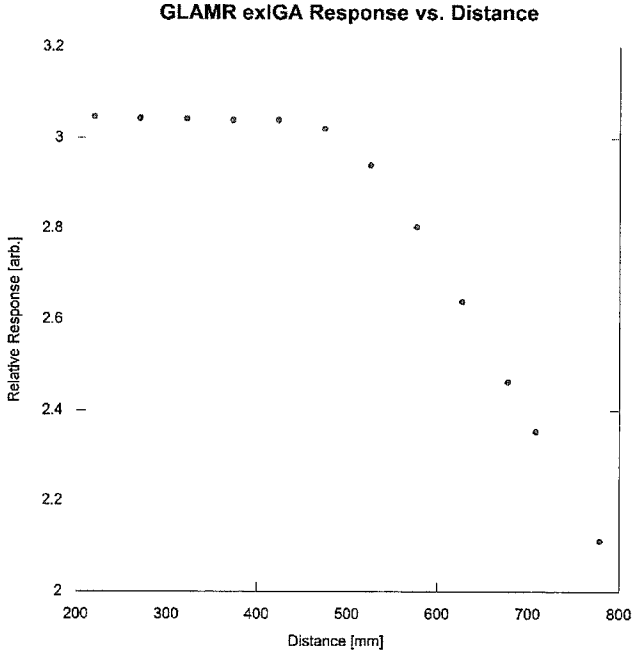

Figure 3.4. Relative response of the exIGA radiometer vs. distance from front aperture to ISS.

3.2 Radiance Responsivity

The optical power response of the GLAMR exIGA radiometer relative to the Gentec pyro, $K(\lambda)$, is shown in Figure 3.5. This can be converted to a relative spectral power responsivity of the GLAMR exIGA using the measured reflectance, $R(\lambda)$, of the Gentec pyro and the assumption that the optical power responsivity of the pyro, $S_{pyro}(\lambda)$, is proportional to 1-$R(\lambda)$, where C_1 is the proportionality constant.

$$S_{xIGA}(\lambda) = C_1 K(\lambda)\big(1 - R(\lambda)\big)$$

Figure 3.6 shows the reflectance of the Gentec pyroelectric detector along with a linear fit to the data. The linear fit was used to obtain $S_{xIGA}(\lambda)$. Figure 3.7 shows the relative spectral power responsivity of the GLAMR exIGA.

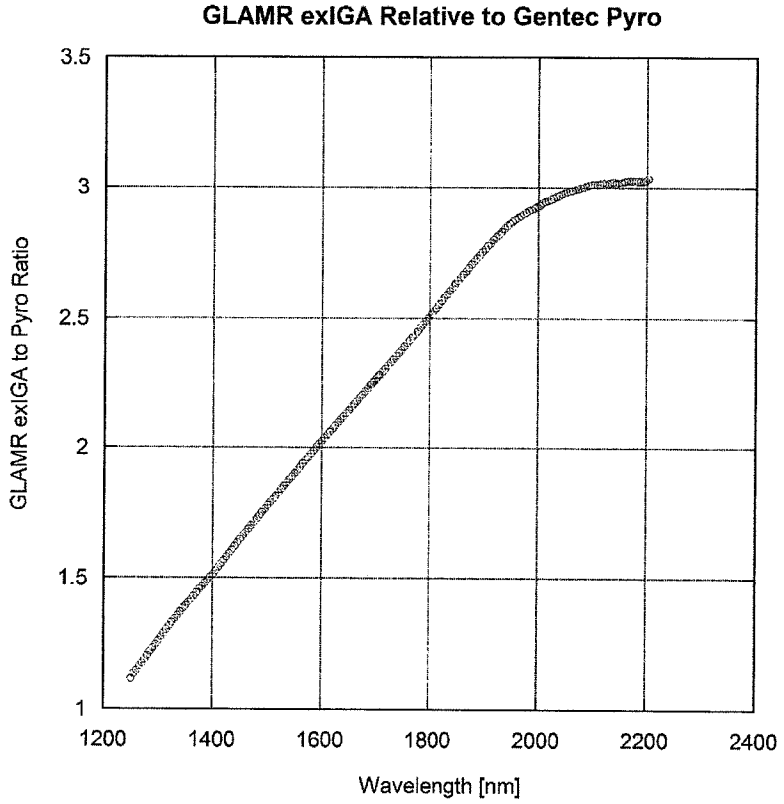

Figure 3.5. The ratio of the optical power response of the exIGA radiometer to the Gentec pyro as a function of wavelength.

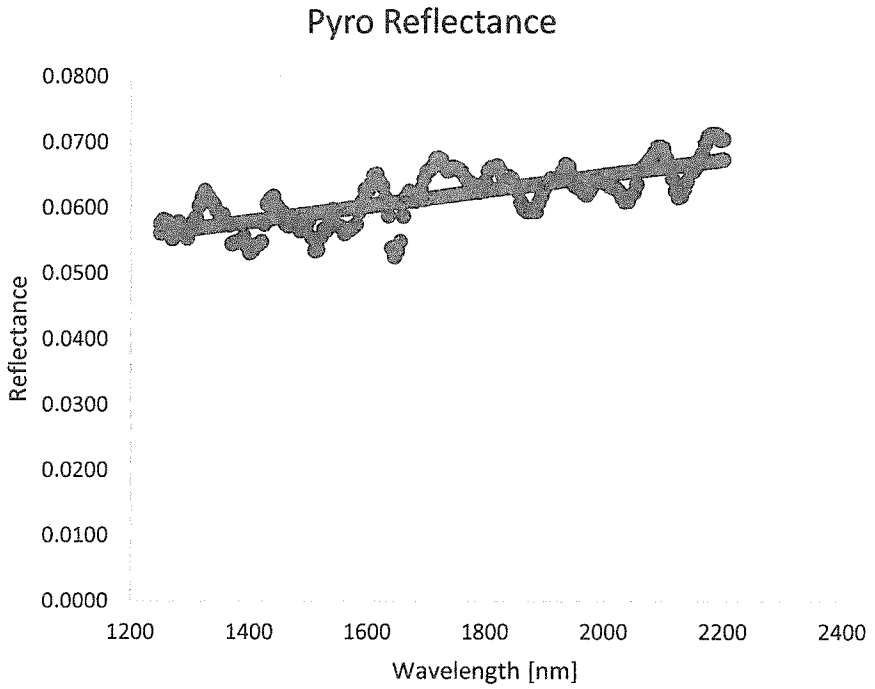

Figure 3.6. Reflectance of the Gentec pyro (red) vs. wavelength and a linear fit (blue).

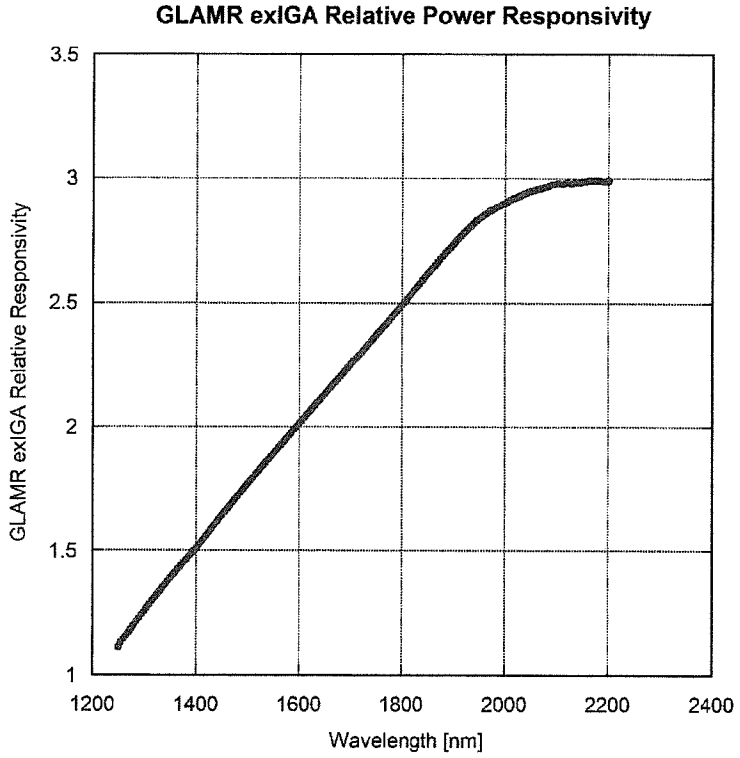

Figure 3.7. Relative power responsivity of the GLAMR exIGA radiometer.

To place the relative power responsivity of the GLAMR exIGA radiometer on the SIRCUS absolute radiance responsivity scale, we scale the relative measurements to the absolute radiance responsivity measurements at 1311 nm, 1402 nm, 1504 nm and 1612 nm made on SIRCUS that were described in section 2.3. Figure 3.8 shows these absolute radiance responsivity data points from SIRCUS as blue circles while the red line shows the relative power responsivity data of Fig. 3.7 scaled to the absolute points. Thus, the red line is the absolute radiance responsivity for the GLAMR exIGA out to 2200 nm.

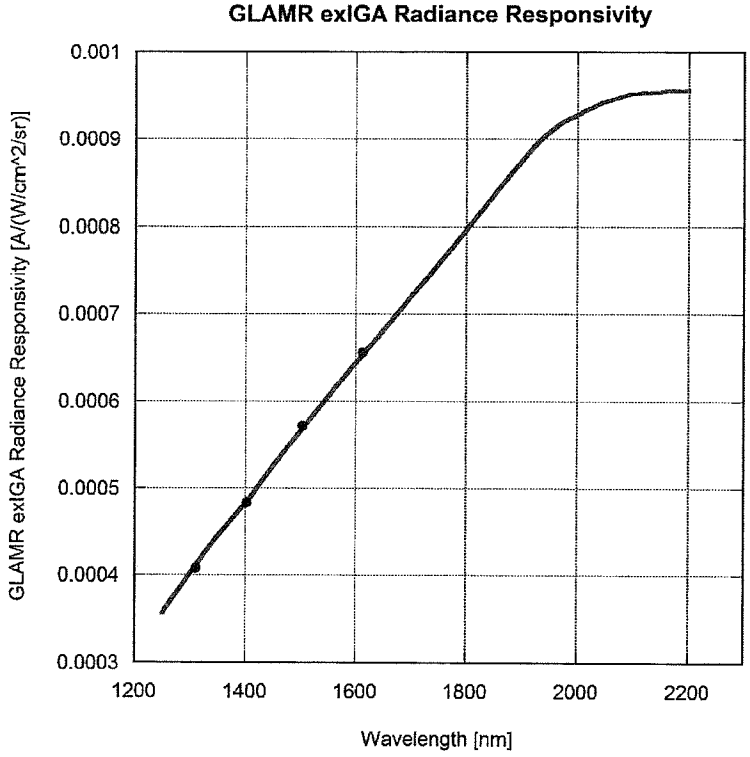

Figure 3.8 Absolute radiance responsivity of the GLAMR exIGA radiometer from 1250 nm to 2200 nm. Blue points are measured on SIRCUS and red line is scaled from Fig. 3.7.

To extend the scale to 2500 nm, we extrapolate the reflectance measurements on the Gentec pyro described in section 2.4 out to 2500 nm and find the corresponding relative responsivity of the Gentec pyro. The radiance responsivity measurements of the GLAMR exIGA relative to the Gentec pyro described in Section 2.3 were then converted to a relative responsivity of the GLAMR exIGA radiometer. In the range 1925 nm to 2200 nm, the relative responsivity of the GLAMR exIGA radiometer was then scaled to the absolute radiance responsivity data shown in Figure 3.8. In Figure 3.9 we show these data as green squares.

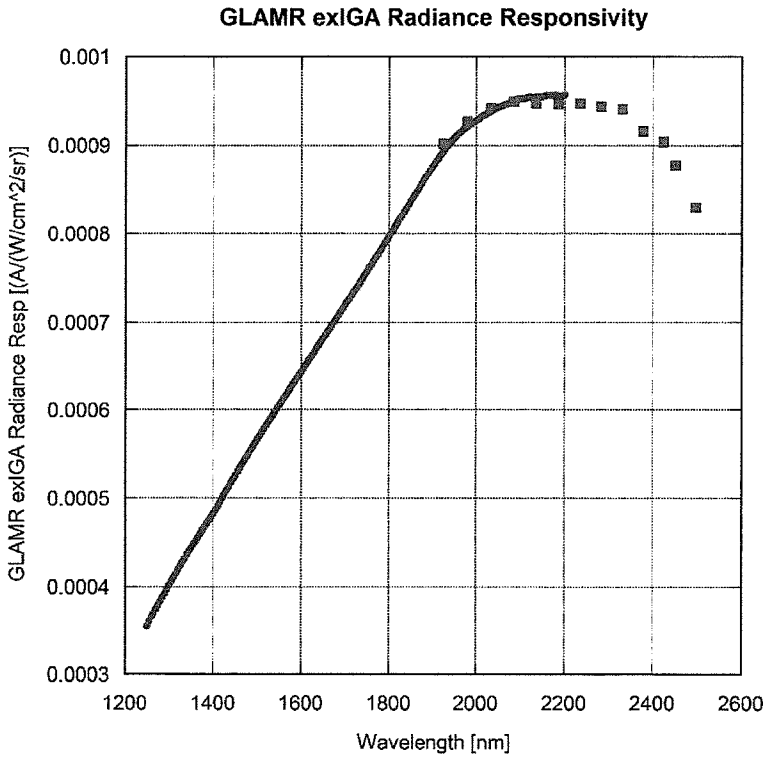

Figure 3.9. Relative GLAMR exIGA radiance measurements (green squares) scaled to the absolute radiance data (red line).

The radiance responsivity was then interpolated to 5 nm intervals with average values taken in the 2100 nm to 2200 nm region. The interpolated data is shown in Figure 3.10 and tabulated below.

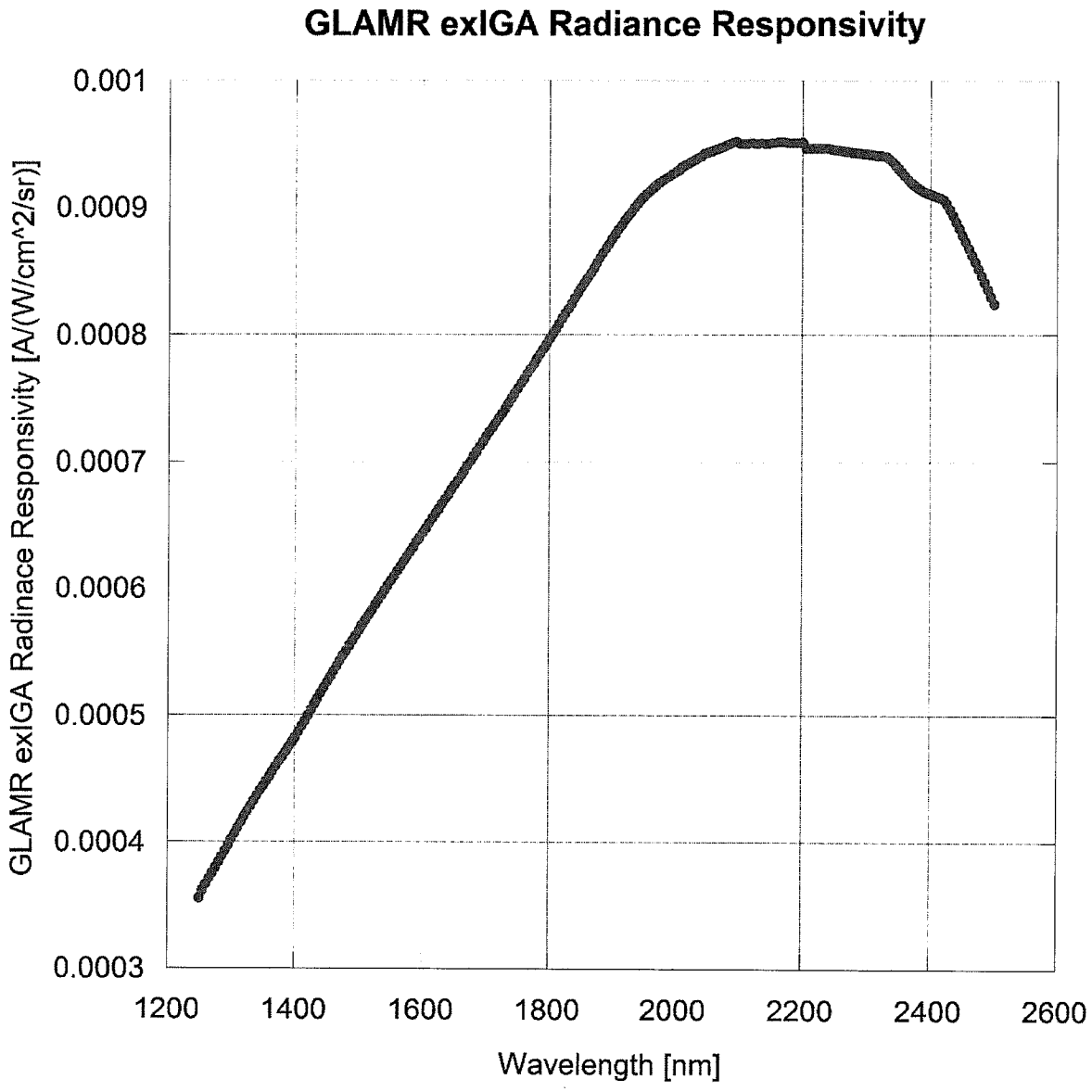

Figure 3.10. Radiance responsivity of the GLAMR exIGA radiometer.

Wavelength [nm]	GLAMR exIGA Radiance Responsivity [A/(W/cm^2/sr)]	% Uncertainty k=1	Wavelength [nm]	GLAMR exIGA Radiance Responsivity [A/(W/cm^2/sr)]	% Uncertainty k=1
1600	6.44E-04	2.1	1795	7.93E-04	2.1
1605	6.48E-04	2.1	1800	7.97E-04	2.1
1610	6.51E-04	2.1	1805	8.01E-04	2.1
1615	6.55E-04	2.1	1810	8.04E-04	2.1
1620	6.59E-04	2.1	1815	8.08E-04	2.1
1625	6.63E-04	2.1	1820	8.13E-04	2.1
1630	6.67E-04	2.1	1825	8.17E-04	2.1
1635	6.71E-04	2.1	1830	8.20E-04	2.1
1640	6.74E-04	2.1	1835	8.24E-04	2.1
1645	6.78E-04	2.1	1840	8.29E-04	2.1
1650	6.82E-04	2.1	1845	8.33E-04	2.1
1655	6.86E-04	2.1	1850	8.37E-04	2.1
1660	6.89E-04	2.1	1855	8.41E-04	2.1
1665	6.93E-04	2.1	1860	8.45E-04	2.1
1670	6.97E-04	2.1	1865	8.48E-04	2.1
1675	7.00E-04	2.1	1870	8.52E-04	2.1
1680	7.04E-04	2.1	1875	8.57E-04	2.1
1685	7.08E-04	2.1	1880	8.61E-04	2.1
1690	7.12E-04	2.1	1885	8.64E-04	2.1
1695	7.16E-04	2.1	1890	8.68E-04	2.1
1700	7.20E-04	2.1	1895	8.71E-04	2.1
1705	7.24E-04	2.1	1900	8.75E-04	2.1
1710	7.27E-04	2.1	1905	8.79E-04	2.1
1715	7.30E-04	2.1	1910	8.83E-04	2.1
1720	7.34E-04	2.1	1915	8.86E-04	2.1
1725	7.38E-04	2.1	1920	8.90E-04	2.1
1730	7.42E-04	2.1	1925	8.93E-04	2.1
1735	7.46E-04	2.1	1930	8.96E-04	2.1
1740	7.50E-04	2.1	1935	8.99E-04	2.1
1745	7.54E-04	2.1	1940	9.03E-04	2.1
1750	7.57E-04	2.1	1945	9.06E-04	2.1
1755	7.61E-04	2.1	1950	9.09E-04	2.1
1760	7.65E-04	2.1	1955	9.11E-04	2.1
1765	7.69E-04	2.1	1960	9.13E-04	2.1
1770	7.73E-04	2.1	1965	9.15E-04	2.1
1775	7.76E-04	2.1	1970	9.18E-04	2.1
1780	7.81E-04	2.1	1975	9.20E-04	2.1
1785	7.85E-04	2.1	1980	9.22E-04	2.1
1790	7.89E-04	2.1	1985	9.23E-04	2.1

Wavelength [nm]	GLAMR exIGA Radiance Responsivity [A/(W/cm^2/sr)]	% Uncertainty k=1	Wavelength [nm]	GLAMR exIGA Radiance Responsivity [A/(W/cm^2/sr)]	% Uncertainty k=1
1990	9.25E-04	2.1	2185	9.51E-04	2.5
1995	9.26E-04	2.1	2190	9.51E-04	2.5
2000	9.28E-04	2.1	2195	9.51E-04	2.5
2005	9.30E-04	2.1	2200	9.52E-04	2.5
2010	9.32E-04	2.1	2205	9.46E-04	2.5
2015	9.34E-04	2.1	2210	9.47E-04	2.5
2020	9.35E-04	2.1	2215	9.47E-04	2.5
2025	9.36E-04	2.1	2220	9.47E-04	2.5
2030	9.37E-04	2.1	2225	9.47E-04	2.5
2035	9.39E-04	2.1	2230	9.47E-04	2.5
2040	9.41E-04	2.1	2235	9.47E-04	2.5
2045	9.42E-04	2.1	2240	9.47E-04	2.5
2050	9.43E-04	2.1	2245	9.46E-04	2.5
2055	9.44E-04	2.1	2250	9.46E-04	2.5
2060	9.45E-04	2.1	2255	9.45E-04	2.5
2065	9.46E-04	2.1	2260	9.45E-04	2.5
2070	9.47E-04	2.1	2265	9.44E-04	2.5
2075	9.48E-04	2.1	2270	9.44E-04	2.5
2080	9.49E-04	2.1	2275	9.44E-04	2.5
2085	9.50E-04	2.1	2280	9.43E-04	2.5
2090	9.52E-04	2.1	2285	9.43E-04	2.5
2095	9.52E-04	2.1	2290	9.43E-04	2.5
2100	9.51E-04	2.5	2295	9.42E-04	2.5
2105	9.51E-04	2.5	2300	9.42E-04	3.0
2110	9.50E-04	2.5	2305	9.42E-04	3.0
2115	9.51E-04	2.5	2310	9.41E-04	3.0
2120	9.51E-04	2.5	2315	9.41E-04	3.0
2125	9.51E-04	2.5	2320	9.41E-04	3.0
2130	9.51E-04	2.5	2325	9.41E-04	3.0
2135	9.51E-04	2.5	2330	9.40E-04	3.0
2140	9.51E-04	2.5	2335	9.39E-04	3.0
2145	9.51E-04	2.5	2340	9.36E-04	3.0
2150	9.51E-04	2.5	2345	9.34E-04	3.0
2155	9.51E-04	2.5	2350	9.31E-04	3.0
2160	9.52E-04	2.5	2355	9.28E-04	3.0
2165	9.52E-04	2.5	2360	9.25E-04	3.0
2170	9.52E-04	2.5	2365	9.22E-04	3.0
2175	9.52E-04	2.5	2370	9.20E-04	3.0
2180	9.51E-04	2.5	2375	9.17E-04	3.0

Wavelength [nm]	GLAMR exIGA Radiance Responsivity [A/(W/cm^2/sr)]	% Uncertainty k=1	Wavelength [nm]	GLAMR exIGA Radiance Responsivity [A/(W/cm^2/sr)]	% Uncertainty k=1
2380	9.15E-04	3.0	2445	8.83E-04	3.0
2385	9.14E-04	3.0	2450	8.78E-04	3.0
2390	9.12E-04	3.0	2455	8.73E-04	3.0
2395	9.11E-04	3.0	2460	8.68E-04	3.0
2400	9.10E-04	3.0	2465	8.63E-04	3.0
2405	9.09E-04	3.0	2470	8.57E-04	3.0
2410	9.09E-04	3.0	2475	8.52E-04	3.0
2415	9.08E-04	3.0	2480	8.47E-04	3.0
2420	9.06E-04	3.0	2485	8.41E-04	3.0
2425	9.03E-04	3.0	2490	8.35E-04	3.0
2430	8.98E-04	3.0	2495	8.30E-04	3.0
2435	8.94E-04	3.0	2500	8.24E-04	3.0
2440	8.89E-04	3.0			

3.3 Radiance Responsivity Uncertainty Analysis

Table 3.1 Uncertainty Budget for Absolute Spectral Radiance Responsivity

	Relative Standard Uncertainty [%]		
Uncertainty Component	**1600 nm to 2100 nm**	**2100 nm to 2300 nm**	**2300 nm to 2500 nm**
Radiance responsivity scale from IGA2017a	1.7	1.7	1.7
Pyro Absorptance	1.0	1.0	1.0
ExIGA to Pyro Ratio 1250 nm to 2200 nm	0.35	0.35	0.35
Scaling Factor 1300 nm to 1600 nm	0.61	0.61	0.61
Extrapolated Pyro Absorptance		1.0	1.5
ExIGA to Pyro Ratio 1900 nm to 2500 nm		0.4	0.61
Scaling Factor 1900 nm to 2200 nm		0.76	0.76
Total k = 1 % Uncertainty	**2.1**	**2.5**	**3.0**

Note 1: A more detailed uncertainty budget is included in the data files provided to the customer. This table includes primary uncertainty components in the designated wavelength ranges.

Note 2: this is not the full calibration uncertainty budget. The uncertainty budget, Table 3.1, does not include environmental effects on both the reference detector and the GLAMR radiometer. There is no component for the wavelength uncertainty. Finally, the uncertainty budget in Table 3.1 does not include measurement uncertainties associated with the GLAMR radiometer itself. No evaluations of instrument performance characteristics such as temperature dependence, response linearity or temporal stability were performed. For estimates in the interpolated uncertainty, refer to Ref. 3.

4. General Information

The integrating sphere used was a LabSphere 30 cm diameter, Spectralon-coated sphere equipped with a 5.00 cm aperture. The distance to the transfer detector was measured radiometrically and fit to an expression for an extended source.

The GLAMR xIGA detector was temperature stabilized. The other detectors are not.

Pyro reflectance measurements were performed by Ping-Shine Shaw.

Relative responsivity measurements from 1200 nm to 2100 nm were performed by Ping-Shine Shaw.

The calibration measurements were performed by John Woodward and Brian Alberding using the VisSIRCUS laboratory and the VisSIRCUS data acquisition program (v10).

Relative responsivity measurements from 1900 nm to 2500 nm were performed by John Woodward and Brian Alberding using the Chopping SIRCUS_V2.vi data acquisition program.

Information was recorded in the SIRCUS Vis #20 laboratory notebook, pp. 61 to 73.

Data were reduced by John Woodward; the uncertainty tables provided were produced by John Woodward.

Tabulated calibration data files were provided along with this report.
Filename: GLAMR_xIGA_Sept2018.xlsx

References

[1] Brown, S. W., Eppeldauer, G. P., and Lykke, K. R., "Facility for spectral irradiance and radiance responsivity calibrations using uniform sources", *Applied Optics* 45 (32) 8218-8237 (2006).

[2] Woodward, J. T, Shaw, P.-S., Yoon, H. W., Zong, Y. Q., Brown, S. W., Lykke, K. R., "Invited article: advances in tunable laser-based radiometric calibration applications at the National Institute of Standards and Technology, USA", *Review of Scientific Instruments* 89 091301 (2018).

[3] Gardner, J. L., "Uncertainties in interpolated spectral data", *Journal of Research of NIST* 108, 69-78 (2003).

Prepared by:

John T. Woodward
Remote Sensing Group, 685.04
Sensor Science Division
Physical Measurement Laboratory
(301) 975-5495

Approved by:

Joseph P. Rice, Leader
Remote Sensing Group, 685.04
Sensor Science Division
Physical Measurement Laboratory
(301) 975-2133